Integrated hydrodynamic-electrical hardware model for wave energy conversion with M4 ocean demonstrator

Judith M. Apsley, Xiaotao Zhang, Iñaki E. Damian, Matteo F. Iacchetti, Zhijing Liao, Peter Stansby, Guang Li, Gangqiang Li, Hugh Wolgamot, Christophe Gaudin, Adi Kurniawan, Xinan Zhang, Zifan Lin, Nuwantha Fernando, Chris Shearer, Brad Saunders

Abstract— **Marine wave energy is a potentially valuable renewable energy resource that can share the same infrastructure as floating wind, with a complementary power delivery pattern. Despite many small-scale sea trials, most previous results are not in the public domain and the technology remains immature. This programme aims to put a 20 m long, kW scale, wave-to-wire multi-modal raft attenuator into the sea in 2023/24, and make datasets ranging from site wave resource surveys to real-time electrical power generation available to researchers. This paper addresses the project design stage, covering the full system integrated hydrodynamic-electrical modelling and hardware specifications for both dry testing and sea trials. The modelling reveals the inter-relationships between the mechanical platform and electrical system constraints. Models are applied to identify the operational limits of the power take-off, particularly the generators, and show how this impacts on total energy extracted with conventional linear damping control. The exercise has identified the energy-storage isolation transformer as under-specified – this is a relatively low-cost item that can be upgraded. The gearbox has emerged as a more significant limiting factor for power scale-up.**

Keywords—**Wave energy, power take-off, simulation, hardware demonstrator.**

I. Introduction

WAVE energy is known to be a renewable energy resource with worldwide capacity similar to wind [1-2]. Potential for multi-MW capacity for grid supply has been demonstrated at many sites but, despite a range of demonstrator sites and devices [3-5], there is to date negligible commercial-scale generation of electricity from wave. Many wave energy converters (WEC) have been proposed [4-6] without convergence on a particular design, as there has been for wind. However, green energy COVID recovery programmes, combined with shortages of natural gas have led to renewed commitment to marine offshore energy [7-11].

This paper addresses a multi-float, articulated attenuator WEC, the Moored Multi-Modal, Multi-float (M4), which has been widely tested in wave basins and modelled by linear diffraction/radiation methods [12-14]. To advance development, a 20 m demonstrator has been designed, which is predicted to give kW-scale power harvesting. Ocean tests are being planned for Albany, Western Australia [11], which has suitable wave conditions for this scale of device. The aim is to learn about aspects of ocean deployment from wave climate and environment planning to realistic electricity generation, albeit at kW scale, and create extensive open access datasets.

In this paper, the emphasis is on the specification of electrical drive train, which acts as the power take off (PTO), converting the movement at the hinge to electrical power. Sizing the PTO for the worst-case sea state is prohibitively expensive, so power-shedding control is required to protect the electrical system. Existing hydrodynamic models have been integrated with Matlab models of the electro-mechanical components, and tested over the range of site conditions, as represented by a scatter diagram. Section II introduces the wave data for the site. Section III briefly reviews the hydrodynamic and electro-mechanical system models and explains constraints on generator and energy storage voltages and

The support of the Western Australian Government, via the Department of Primary Industries and Regional Development (DPIRD), and the Blue Economy Cooperative Research Centre through the project 'Seeding Marine Innovation in WA with a Wave Energy Deployment in Albany' is gratefully acknowledged. The Blue Economy Cooperative Research Centre (CRC) is established and supported under the Australian Government's CRC Program, grant number CRC-20180101. This work was also supported by the UK Engineering and Physical Sciences Research Council under grant EP/V0405101/1 Judith Apsley (j.apsley@manchester.ac.uk), Xiaotao Zhang, Zhijing Liao, Peter Stansby, Guang Li and Gangqiang Li are at the School of Engineering, University of Manchester, Matteo Iacchetti is with the University of Manchester, and with Politecnico di Milano, UK. Inaki Damian was at the School of Engineering, University of Manchester, UK and is now at Schlumberger, Bristol, UK. Hugh Wolgamot, Christophe Gaudin, Adi Kurniawan, Xinan Zhang and Zifan Lin are at the Oceans Graduate School, University of Western Australia, Australia, Nuwantha Fernando is at RMIT, Melbourne, Australia. Chris Shearer and Brad Saunders are at BMT, Australia.

Digital Object Identifier: https://doi.org/10.36688/ewtec-2023-500

currents. Section IV reviews the full system design including instrumentation. Section V evaluates the power recovery subject to constraints. Conclusions evaluate the power-limiting control, and identify the limiting factors.

II. SITE CONDITIONS

Wave buoy data are available for the proposed site in King George Sound, Western Australia. Sea-state data for summer wave conditions on the site are shown in the scatter diagram in Fig. 1, from [15]. The most likely occurrences have mean periods in the range 3-7 s. The significant wave height H_s and peak period T_p are used as inputs to generate wave-forcing functions in the models, following, e.g. [12, 13].

The M4 platform performs optimally in terms of power generation with a T_p of 3.5 s or mean period of about 3 s. Sea states with larger mean period are off resonant while still generating significant power. The average H_s is about 0.5 m with a low probability of 1.25 m and above. Electrical component costs scale with both voltage and current, so it is not cost effective to size the PTO for high sea states, since the total energy recovered is low. However, the PTO still has to be designed to survive these conditions.

On some WECs, mechanical protection has been used such as end stops. In the M4 platform, submersion of the floats occurs in high sea states, and this dunking action restricts the hinge motion to ±45°, passively protecting the platform. This occurs above the electrical power rating of the PTO, which is further protected by setting the power generated to zero.

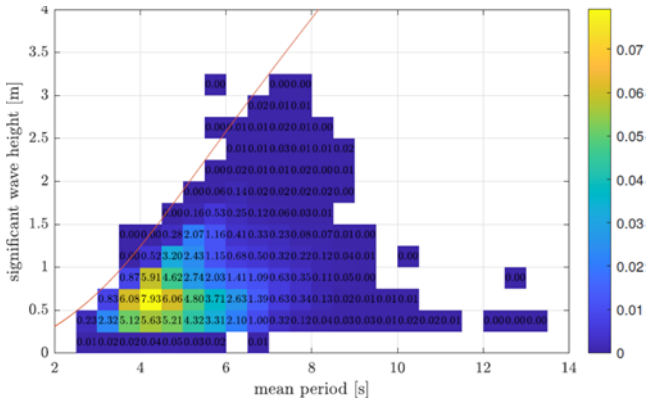

Fig. 1 Scatter diagram showing occurrence of significant wave height and mean period combinations for summer wave conditions at the King George Sound site, from [15].

III. SYSTEM MODELS

The full wave energy system is shown in Fig. 2, which encompasses the hydrodynamic, electro-mechanical and control elements. Hydrodynamic system models were initially developed in FORTRAN for the analysis and design of the WEC platform and were extended and transferred to Matlab for evaluation of real-time control strategies for maximum extraction. These have been validated on a range of 2 m long prototypes in tank tests, through to the mechanical power take-off.

The electrical PTO has been modelled in Matlab to allow initial sizing of the full wave-to-wire platform. The PTO includes a permanent magnet (PM) generator, a super-capacitor for power smoothing, and a resistive load, for power dissipation, each with their associated power electronic converter. The need for power smoothing is widely covered in the literature, and super-capacitors are the most common choice of energy storage component [16-19].

PM machines are the dominant technology in applications ranging from wind turbines to electric vehicles. [16-19] all use PM generators, due to their low loss and large airgap. The induced voltage of a PM generator is proportional to its speed. In [20], field weakening is used to manage the terminal voltage, preventing damage to the power electronics and demonstrating a reduction in the levelized cost of energy. With field weakening, torque reduces as speed increases.

In extreme sea states, the M4 PTO is disabled by disconnecting the generator from the power converter, which sets the current to zero. The generator insulation must be rated to withstand the high open-circuit terminal voltages. Protection through open-circuit was preferred to the alternative of shorting the generator terminals, since in the latter mode the generator must be continuously rated for the resulting short-circuit current. Whilst it is possible to design machines with low short-circuit current [21], such machines generally have a poor power factor and lower efficiency.

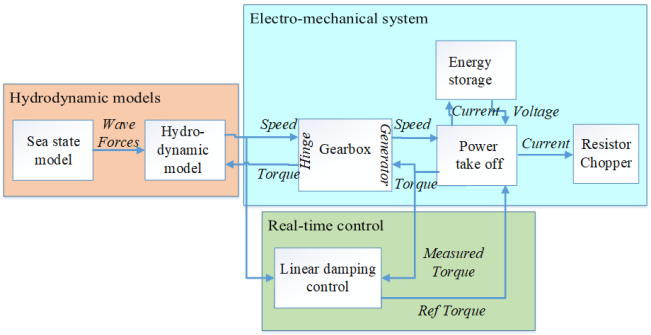

Fig. 2 System overview

1) *Hydrodynamic models*

The hydrodynamic modelling of the M4 platform has been reported extensively in [12-14], which include tank test validation. Key equations are summarised below but readers are referred to [13] for further details of the state space modelling.

The motion vector is defined as $q = [x_o,\ z_o,\ \theta_l,\ \theta_r]^T$ where x and z represent surge and heave motion of the hinge point, while θ_l and θ_r stand for the pitch motion of the front and rear sections with respect to the hinge. The relative pitch, $\theta = \theta_l - \theta_r$, is the angular rotation driving the generator. The equation of motion based on linear wave theory is:

$$M\ddot{q} = f_{e,q} + f_{rd,q} + f_{rs,q} + f_{pto,q} \quad (1)$$

where M is the mass and inertia matrix, $f_{e,q}$ is the excitation force, $f_{rd,q}$ is the radiation force, $f_{rs,q}$ is the hydrostatic and gravitational restoring force and $f_{pto,q}$ is the torque T_e provided by the generator, acting through a gearbox with ratio g.

$$f_{pto,q} = [0 \quad 0 \quad -gT_e \quad gT_e]^T \tag{2}$$

The radiation force is modelled using Cummins' method and used to derive some state-space sub-systems. The equation of motion can be rewritten as:

$$(M + m_\infty)\ddot{q} - f_{rd,q} + Kq = f_{e,q} + f_{pto,q} \tag{3}$$
$$\dot{z_s} = A_s z_s + B_s \dot{q} \tag{4}$$
$$f_{rd,q} = C_s z_s + D_s \dot{q} \tag{5}$$

where m_∞ is the infinite frequency added mass matrix, K is the restoring stiffness matrix, z_s the auxiliary state for radiation sub-systems, and A_s, B_s, C_s, D_s are the state-space matrices.

The state-space model built from the equation of motion by introducing a state vector $x = [q,\ \dot{q},\ z_s]^T$ takes the form:

$$\dot{x} = Ax + B(f_{e,q} + f_{pto,q}) \tag{6}$$
$$y = Cx \tag{7}$$

where output y is the platform rotational velocities.

Writing $M_1 = M + m_\infty$, and n as the selected model order for the radiation sub-system, system matrices are given by:

$$A = \begin{bmatrix} 0_{4\times4} & I_{4\times4} & 0_{4\times n} \\ -{M_1}^{-1}K & -{M_1}^{-1}D_s & -{M_1}^{-1}C_s \\ 0_{n\times4} & B_s & A_s \end{bmatrix} \tag{8}$$

$$B = \begin{bmatrix} 0_{4\times4} \\ {M_1}^{-1} \\ 0_{n\times4} \end{bmatrix} \tag{9}$$

$$C = [0_{1\times4}, 0,0,1,-1, 0_{1\times n}] \tag{10}$$

2) Platform Control

The focus of this project is to gain sea trial experience for the wave energy platform. For this reason, protection has been prioritised over power-optimised control. Hence, initial sea trials will use standard linear damping control. As shown in Fig. 2, the mechanical platform sets the speed of the generator, where $\omega_g = g\dot{\theta}$. This speed is used in the controller to set the reference torque, denoted with *. In the motoring conventions used throughout the paper, the negative sign indicates generation (power out).

$$T_e^* = -k_{pto}\omega_g \tag{11}$$

There are constraints on PTO current and voltage, which may prevent generator torque from following its reference so actual torque is fed back through the gearbox to the platform model. It is also fed back to the controller for future development of constraint-limited control strategies. Further information on PTO constraints is presented in the next section.

3) Electrical system models

Matlab models have been created for the PTO to represent the PM generator and its converter and the super-capacitor energy storage. The PM generator analysis uses a second-order non-linear state space model in the synchronous reference frame assuming an isolated star connection and using motoring conventions.

$$\frac{di_d}{dt} = \frac{1}{L_d}\left(v_d - Ri_d + L_q\omega_e i_q\right) \tag{12}$$
$$\frac{di_q}{dt} = \frac{1}{L_q}\left(v_q - Ri_q - L_d\omega_e i_d - \psi_m\omega_e\right) \tag{13}$$
$$T_e = p[\psi_m i_q + (L_d - L_q)i_q i_d] \tag{14}$$

Where v is voltage, i is current, ψ_m is magnet flux linkage, $\omega_e = p\omega_g$ is angular electrical speed, p is pole pairs, R is resistance, and L is inductance. Subscripts dq refer to the synchronous axes, with the constant power transform. Saliency, saturation, thermal variations, iron loss and mechanical loss are neglected.

The generator uses conventional field oriented control, based on measured angular position, with proportional-integral (PI) current control. Under normal operation, field weakening current is zero and torque current is derived from reference torque, based on (11) and (14).

If the generator peak line-line voltage exceeds the converter DC voltage v_{dc}, it is no longer possible to control the generator torque. This could result in failure of the power converter, generator and gearbox. The generator voltage constraint is given in (15), assuming space vector modulation.

$$0 \le \sqrt{v_d^2 + v_q^2} < \frac{v_{dc}}{\sqrt{3}} \tag{15}$$

However, field-weakening current i_d can be used to reduce the generator terminal voltage; see [22] for full details of the algorithm. Too much current can result in catastrophic failure of windings and power electric devices, so there are also constraints on the current, where I_{max} is determined by the lesser of the generator or inverter current limits.

$$-I_{max} < i_d^* \le 0 \tag{16}$$
$$\left|i_q^*\right| \le \sqrt{I_{max}^2 - i_d^{*2}} \tag{17}$$

The platform spans multiple timescales, from a 3-hour sea state, to sub millisecond electrical time constants, so in practice, reduced order models of the PTO have been developed [23] to be suitable for both design optimisation and real-time predictive control. In these models,

differential terms in (12) and (13) are neglected and the converter is modelled using power balance.

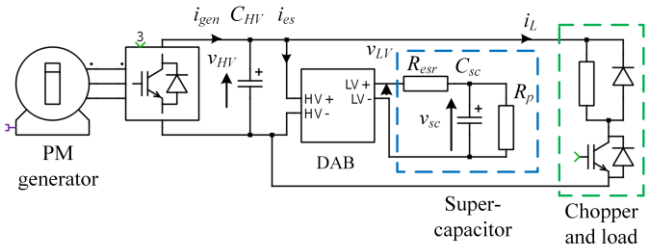

Fig. 3 PTO electrical circuit; mechanical and gating signals have been omitted for clarity

The DC circuit is shown in Fig. 3. The demonstrator is a standalone system with super-capacitor energy storage C_{sc} which is interfaced to the DC bus with a bi-directional isolated dual active bridge (DAB) converter [18]. The DAB converter uses a single PI controller to regulate the DC link voltage, with tuning transfer functions based on [24]. Whilst full circuit modelling has been used for controller development, in this paper, DC link voltage regulation is treated as ideal, so high frequency power fluctuations are exchanged with the super-capacitor P_{sc}, whilst the chopper acts in current control mode to dissipate the average power P_R in the load.

Power flow is managed with a low pass filter with time constant τ_f according to [18], where the low frequency term is fed to the load resistor (18), and the high pass term to the super-capacitor (19), where s is the Laplace operator.

$$P_R = \frac{P_{gen}}{1 + s\tau_f} + P_{xs} \tag{18}$$

$$P_{sc}^* = \frac{s\tau_f P_{gen}}{1 + s\tau_f} \tag{19}$$

Desired super-capacitor current i_{sc}^* can be related to the voltage v_{sc} and power transferred across the DC/DC converter through power balance (20). Solution of the quadratic simplifies to (21), due to the low value of equivalent series resistance R_{esr}.

$$P_{sc}^* - i_{sc}^* v_{sc} - i_{sc}^{*2} R_{esr} = 0 \tag{20}$$

$$i_{sc}^* \approx \frac{P_{sc}^*}{v_{sc}} \tag{21}$$

To prevent saturation of the transformer in the DAB, there is a constraint on super-capacitor current, I_{sclim}:

$$i_{sc} = lim\{i_{sc}^*\}, where\ -I_{sclim} < i_{sc}^* \leq I_{sclim} \tag{22}$$

The actual current will charge capacitance C_{sc} with leakage path resistance R_p:

$$\frac{dv_{sc}}{dt} = \frac{1}{C_{sc}}\left(i_{sc} - \frac{v_{sc}}{R_p}\right) \tag{23}$$

To prevent over-voltage of the DC link, any additional power P_{xs} has to be dissipated.

$$P_{xs} = P_{sc}^* - i_{sc}(v_{sc} + R_{esr} i_{sc}) \tag{24}$$

The excess power is passed to the load resistors (18). To extend super-capacitor lifetime, a limited voltage range from $V_{sc,min}$ to $V_{sc,max}$ is defined:

$$V_{sc,min} < v_{sc} \leq V_{sc,max} \tag{25}$$

In practice, a small additional current is required by the super-capacitor to maintain its average state-of-charge, which is managed by a proportional-only controller.

IV. FULL SYSTEM DESIGN

1) *Platform*

The mechanical platform is shown in Fig. 4. The platform measures approximately 20 m in length by 9.5 m wide. The 1-2-1 configuration has a single bow float (purple), two central floats (red), and a single stern float (yellow). As waves propagate along the platform the forces on bow/mid/stern floats experience different phases exciting rotation at the hinge points. The forces are principally heave and surge. Because both hinge points connect to the same front and rear sections, the speed is the same at both take-off points. This gives a low-speed, high torque reciprocating rotary motion.

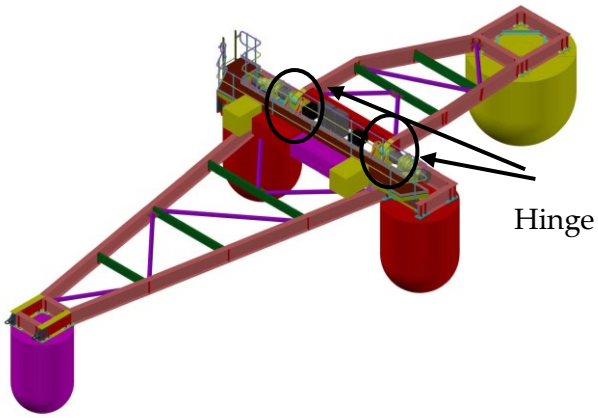

Fig. 4 CAD image of the 121 M4 wave energy platform from BMT

The platform is constructed from steel, with the hollow floats containing ballast. Dimensions and mass distribution have been designed to provide sufficient buoyancy, stability and structural strength [14]. The WEC is moored by a tether to a fairlead on the bow float.

2) *Power take-off*

The electrical power take-off for one of the two identical channels is illustrated Fig. 5. Components are:

1) A high ratio 739:1 (WEC:generator) gearbox,
2) An off-the-shelf permanent magnet generator, which gives three-phase variable voltage, variable frequency AC outputs.
3) Switchgear to protect the converter from high voltages at excessive speeds
4) An AC/DC power electronic converter, which provides closed-loop control of the generator torque-

producing current, with additional field weakening at high speeds as outlined in section 2.3.

5) A DC breaker to connect the converter to the 600 V DC circuit
6) Filter capacitors to stabilise the DC voltage.
7) A dual active bridge DC/DC converter, which interfaces with the super-capacitor energy storage to regulate the 600 V DC circuit.
8) The super-capacitors, which provide power smoothing by exchanging energy with the DC circuits
9) A chopper circuit.
10) A resistor bank. This act with the chopper circuits as a variable resistance load for dissipating the generated energy.
11) A centralised controller.

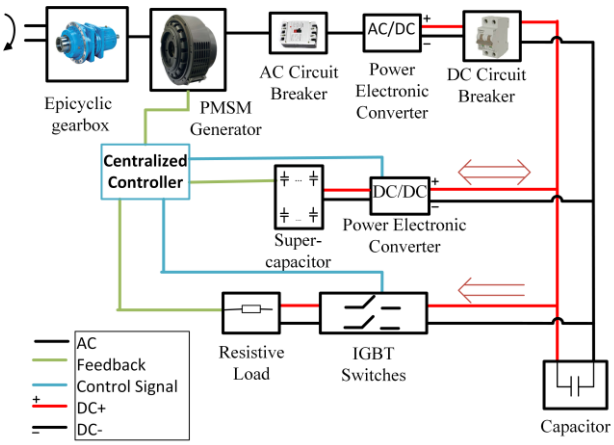

Fig. 5 Electric system overview of a single channel.

Corresponding part numbers, parameters and constraints are listed in Table 1. Items 4, 5, 6, 7 and 9 are rack-mounted power electronic prototyping cards, which interface with the RTU box control board, item 11, and are supported by Simulink library blocks allowing code-generation from Simulink. This allows full flexibility for control of start-up and shut-down sequences, and adjustment of protection limits and tuning gains. Procurement of the PTO highlighted challenges with the gearbox, which would make scale-up to higher powers difficult. Very few suppliers could provide a gearbox with such a high gear ratio, combined with the high torque capability. Higher torque would require larger gears, but clearance distances need to be preserved to ensure equal power sharing between gears and minimise backlash, leading to very demanding tolerances on manufacturing.

Table I gives both the generator nominal continuous rating and derived constraints. The generator has a high peak-to-mean duty and typically is rated for rms torque rather than peak torque, so the DC/AC converter has been sized to allow a short-term overload of twice rated current. Voltage and speed constraints are calculated based on 600 V operation, rather than the 800 V limit. The Siemens generator replaces the generator listed in Table II, because the inertia of the old generator was too large, resulting in overload of the gearbox during rapid acceleration and deceleration. Both generators are compared in Section V.

TABLE I
PTO COMPONENTS, PARAMETERS AND CONSTRAINTS

Description	Part Number	Constraints	Parameter
Gearbox	Boneng P3SA, 11,	42 kNm	95% efficiency
Generator	Siemens Simotic 1FK7103-2AC74-1AA1	[1]38.1A pk dq [1]424.2 V pk dq [1]10,300 rpm [2]11 A rms [2]400 V rms [2]5.5 kW [2]2000 rpm	Rs, 0.29 Ω Ld, 7.9 mH Lq, 7.9 mH k_T, 2.45 NmA^{-1} 4 pole pairs ψ_m, 0.386 Vs J, 0.0104 kgm^2
AC/AC converter	EC6304D0G-43A	[2]14 A rms [2]380 V rms	30 kHz
DC/AC converter	RTM-PEH8025IF	[2]25 Arms 800 V DC	20 kHz
Capacitor board	RTU Cap	800 V DC 2.1 A ripple	4 mF
DC/DC converter	RTM-PEH8035SF	800 V 35 A DC	200 kHz
Trans-former	Custom	300:600 V 20:10 A DC	-
Super-capacitor	MK-270V-P27FLJM	[2]20 A DC 270 V DC	27 F 38 mΩ
Chopper	Infineon FF600R12ME4	800 V, 600 A	-
Resistor	Wirewound, porcelain	-	500 Ω, 3 kW each
Controller	RTU Box 206	-	10 µs

[1]Derived from motor data assuming 600 V DC system, [2]Continuous

TABLE II
PREVIOUS GENERATOR PARAMETERS AND CONSTRAINTS

Description	Part Number	Constraints	Parameter
Old Generator	SMP300XS-45-01	[1]35.33 A pk dq [1]424.2 V pk dq [1]3100 rpm [2]10.2 A rms [2]415 V rms [2]6 kW [2]1500rpm	Rs, 0.1442 Ω Ld, 3.27 mH Lq, 5.75 mH k_T, 3.745 NmA^{-1} 8 pole pairs ψ_m, 0.270 Vs J, 0.1646 kgm^2

[1]Derived from motor data assuming 600 V DC system, [2]Continuous

3) *Sensing and instrumentation*

As listed in Table III, sensing is embedded into the real-time platform for control and protection. This primarily consists of voltage and current sensing in the power electronic components. Absolute angular position sensing of the generator shaft is a fundamental requirement for the control. Additional instrumentation and data logging will be provided for long-term evaluation of performance, with upload to shore. Further monitoring may be added as budget allows, particularly vibration and strain at locations in the hull, mechanical shaft torque, and temperature of power electronic components. For a 3-7 s mean wave period, long term monitoring will log data at a 100 ms update rate.

Sea state information is initially required to evaluate system performance. Weather data will be used to shut down the PTO remotely if high sea states are expected. Longer term, there would be scope to use real-time sea-state data for advanced optimal power control methods.

TABLE III
SENSING AND INSTRUMENTATION

[1]Use	Description	Sensors	Measurands
M/C/P	Ocean waves	Wave buoy	Height, Period Direction.
M	Wind	Anemometer	Speed, Direction.
M	Mooring	Load cell	Cable tension.
M	Hull	Inertial measurement unit	Orientation, Acceleration
M	PTO (mechanical)	Strain gauge Encoder	Torque. Hinge angle, Speed.
M/C	Generator	Position sensor Current	Absolute position, Speed, Estimated torque, Flux current.
M/C/P	AC/DC converter	Integrated current & voltage	DC current, DC voltage, Recovered power.
C/P	DC/DC converter	Integrated current & voltage	Current, High side voltage, Power.
M/C/P	Super-capacitor	Voltage	DC voltage
M/C/P	Resistor/Chopper	Current	Recovered power.

[1]M= monitor, C= control, P=protection

V. CONSTRAINT LIMITED POWER RECOVERY PREDICTION

This section presents simulation results for a single active channel activated in typical sea states, with some power limiting. Since the plan would be to continue to log data at sea even if one PTO failed and this represents a worst case operation. In these models, the DC voltage control has been treated as ideal. To protect the gearbox, high side torque is constrained to 51.15 Nm.

1) *Effect of constraints*

Fig. 6 shows PTO waveforms for 30 s of an above-average sea-state with T_p= 4.2 s and H_s= 1.0 m, with the old generator, to illustrate the effect of the constraint-limited control. Below 991 s and above 1016 s, torque is linearly related to speed, due to the linear damping (11). Both waveforms have the same shape, but the torque is inverted. These regions are within the constraints, so field weakening current i_d is zero, and torque current i_q is proportional to the torque. Power is the product of torque and speed, so gives a double-frequency fluctuation.

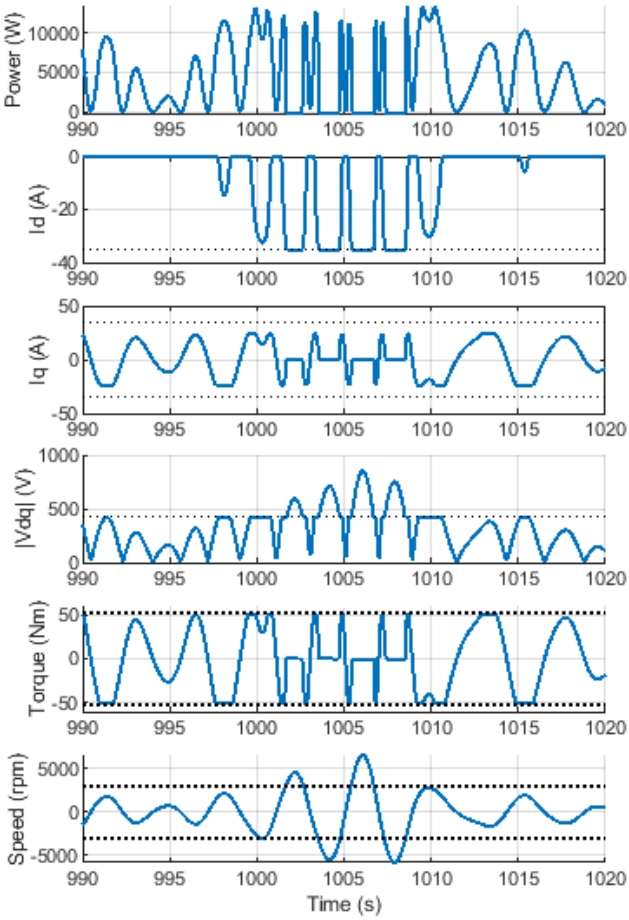

Fig. 6 Effect of constraints (dashed lines) on PTO with old generator on power recovery; from top (blue lines): electrical power, generator field weakening current i_d, torque current i_q and voltage magnitude $|v_{dq}|$, generator torque and speed.

At 991 s the negative torque limit of the gearbox is reached. The control correctly limits the torque, so both torque and torque current are flat until 992 s when the wave subsides and the torque magnitude reduces again. The speed constraint is not reached and the field weakening current remains zero. This represents the first level of power limiting, through torque limiting. For the UWA demonstrator, this limit was defined by the need to protect the gearbox.

In the region from 997.7 s to 998.5 s, the voltage limit of the generator is reached. The control injects field weakening current i_d, to limit the voltage, so the voltage trace is flat. Between 1000s and 1001 s, it can be seen that the torque current i_q has to be reduced, in order to meet the current constraint, so both torque and power reduce. This represents the second level of power limiting, through voltage limiting.

In the extreme case, for example between 1006 s and 1007 s, the field-weakening limit of the generator is reached. The converter current is all field cancelling current, i_d, there is no torque current i_q, and hence no torque, so no power is generated. It can be seen that the voltage magnitude exceeds the voltage limit. This would require immediate intervention to protect the power converter, either by shorting the generator terminals, or by disconnecting the generator. In the demonstrator, the latter

method is preferred since the generator is not rated to withstand the short-circuit currents. A contactor has been fitted for this reason. This represents system shutdown.

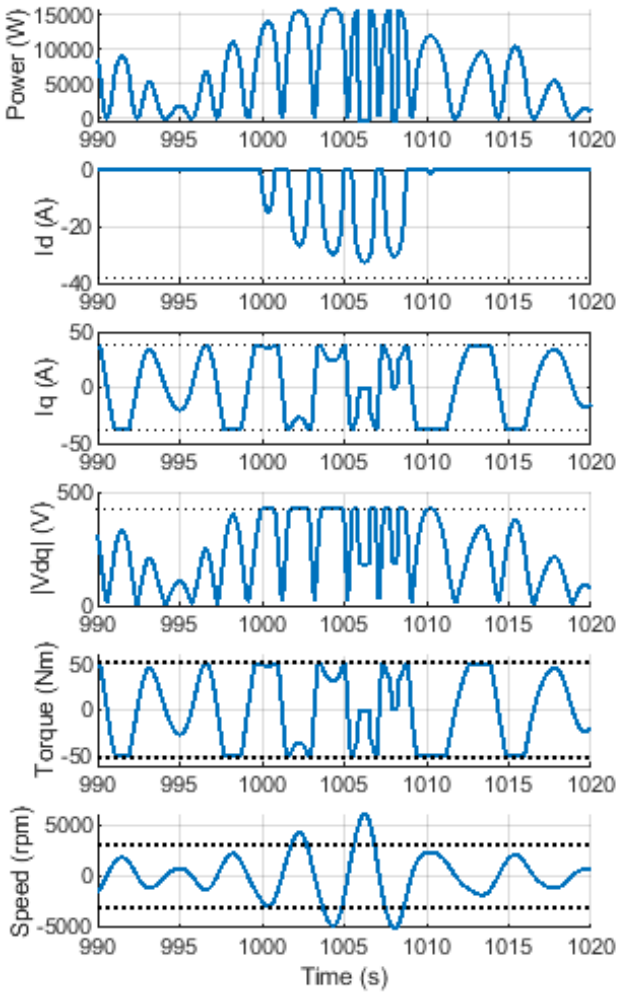

Fig. 7 Effect of constraints (dashed lines) on PTO with new generator on power recovery; from top (blue lines): electrical power, generator field weakening current i_d, torque current i_q and voltage magnitude $|v_{dq}|$, generator torque and speed.

The amount of speed range extension due to voltage limiting depends on the design of the generator [20] and gives trade-offs between speed range and power factor. Fig. 7 shows PTO waveforms for the same excitation force-time profile as Fig. 6, but with the new generator. In Fig. 7, torque limiting is also encountered at 991 s, where both the torque and current i_q traces become flat-topped. The duration of torque limiting is longer due to the lower torque constant of the new generator. Voltage limiting applies over the same part of the waveform in both generators, but the amount of field-weakening current i_d is lower in the new generator, and so the reduction in torque current i_q is smaller. Unlike in Fig. 6, the field-weakening current i_d does not reach its limit. However, torque current is still set to zero, for example between 1006 and 1007 s, but this is because the generator has reached its datasheet maximum speed of 5000 rpm, rather than due to the voltage limit. The shutdown prevents excessive losses due to the over-speed.

Fig. 8 shows corresponding energy storage and resistive load waveforms for the same 30 s section of the same sea state as Fig. 7, to illustrate the effect of the constraint-limited control on the energy storage. The power-sharing control has been set with a τ_f=10s filter constant, so that slowly varying currents are passed through to the load, but fluctuations at the wave cycle frequency are absorbed by the energy storage. It can be seen that below 1000 s and above 1010 s this strategy is working correctly. The 4.7 kW average power (averaged over for the full 20 min test duration) is delivered to the resistors, and the super-capacitors manage the power fluctuations. The super-capacitor voltage fluctuation is less than 7 V, which is acceptable, and the magnitude is below the 270 V limit.

However, although the DC/DC converter has a 35 A limit, its isolation transformer has a 20 A low side current limit. Between 998 s and 1020 s, this limit is reached repeatedly. Grid standards do not allow this sort of power fluctuation, so normally this power would have to be discarded, usually into a dump resistor. For simplicity, in the demonstrator this additional power has been passed through to the resistor load. Hence, the resistor current shows fluctuations whenever the super-capacitor goes into current limiting mode.

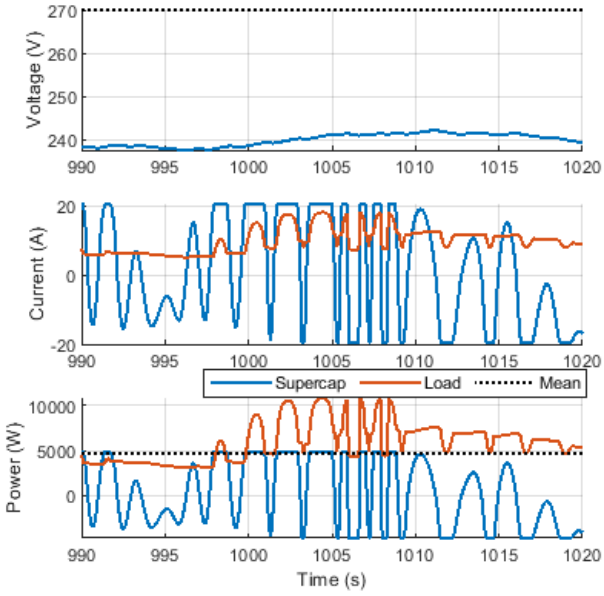

Fig. 8 Effect of energy storage constraints on power recovery, from top: super-capacitor voltage v_{sc}, super-capacitor and load currents, super-capacitor and load power.

The model over-predicts this behaviour, since gearbox converter and generator iron losses have been neglected, due to lack of data. However, it would be better to match the power limits of the energy storage system, including the isolation transformer, with those of the generator. This is a relatively low-cost item that can be upgraded. Initial calculations were done for a full state-of charge, whereas it is usual to run the energy storage for some safety margin on state of charge.

2) Evaluation of power recovery.

The simulation was run for a ≈20 min duration with a wave period T_p of 4.2 s for three different sea states, with a wave height H_s of 0.5 m, which is a probable operating condition, 1.0 m (still likely) and 1.25 m (extreme), referred to as normal, high and extreme respectively.

Figs. 9-11 show power and energy at the top, with generator electrical parameters, field weakening current i_d, torque current i_q and voltage magnitude below. Dashed lines indicate limits. Since the gearbox is the limiting factor, torque is shown across the gearbox, and speed is for the platform side, although the speed limit is imposed by the generator. Energy values assume that operation will resume as soon as the over-speed condition is removed, which is the most optimistic scenario. In practice, sea trials will be much more conservative than this, and the generator will not be reconnected until the sea state has reduced.

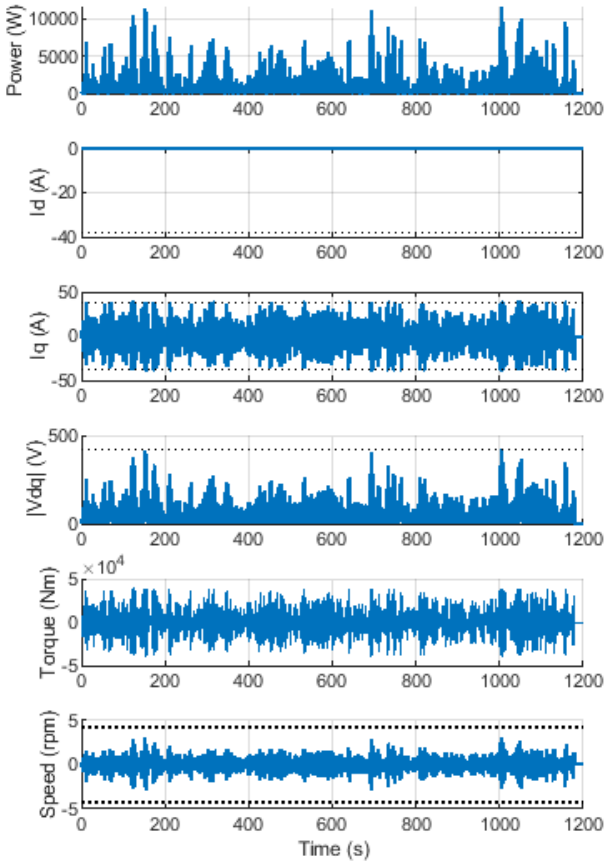

Fig. 9 PTO operation at normal conditions, from top: electrical power, generator field weakening current i_d, torque current i_q and voltage magnitude, gearbox torque and hinge speed.

Fig. 9 shows that in the normal sea state, torque limiting is applied occasionally (i_q reaches its limit), but field weakening is not triggered (no dips in i_d, although voltage comes close to the limit), and no speed violations occur. Average power is 1.39 kW, with a peak/mean power ratio of 11.3.

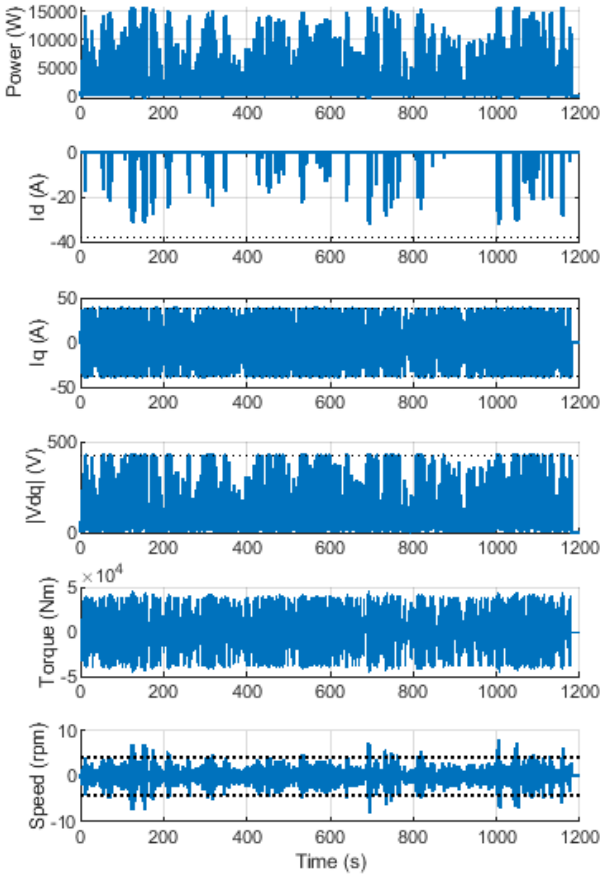

Fig. 10 PTO operation at high conditions, from top: electrical power, generator field weakening current i_d, torque current i_q and voltage magnitude, gearbox torque and hinge speed.

Fig. 10 shows that in the high sea state, torque limiting is applied regularly (i_q reaches its limit), and field weakening is triggered quite frequently (dips in i_d). Six speed violations occur in the 20 min period, but speed excursions are small. The challenge in the sea trials will be to manage these speed violations and keep the platform operational. Average power is approx. 4.72 kW with a peak/mean power ratio of 3.34.

Fig. 11 shows that in the extreme sea state, torque limiting is applied on most wave cycles and field weakening is triggered regularly. Frequent speed violations occur in the 20 min period. The recommendation would be to disconnect the generator in this sea state. Average power of 6.12 kW is above the generator rating and is not sustainable.

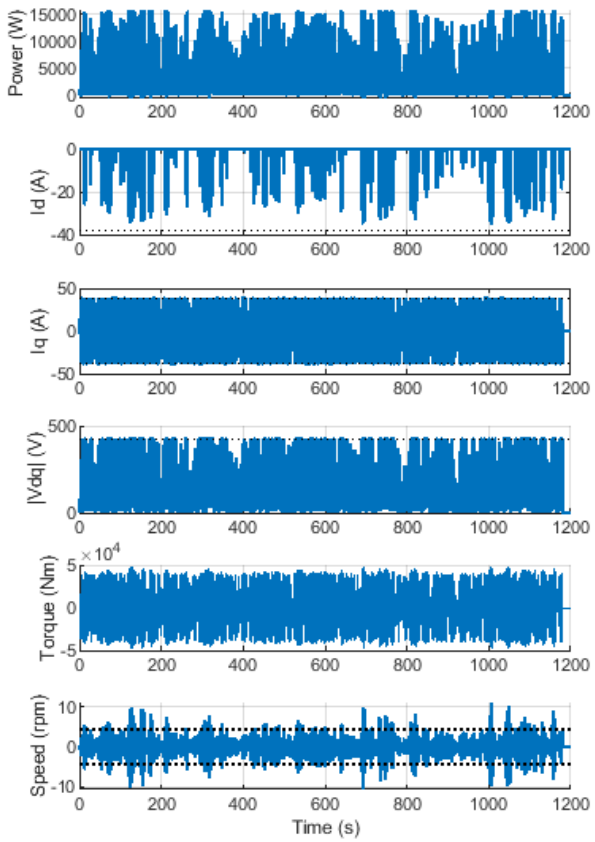

Fig. 11 PTO operation at extreme conditions, from top: electrical power, generator field weakening current i_d, torque current i_q and voltage magnitude, gearbox torque and hinge speed.

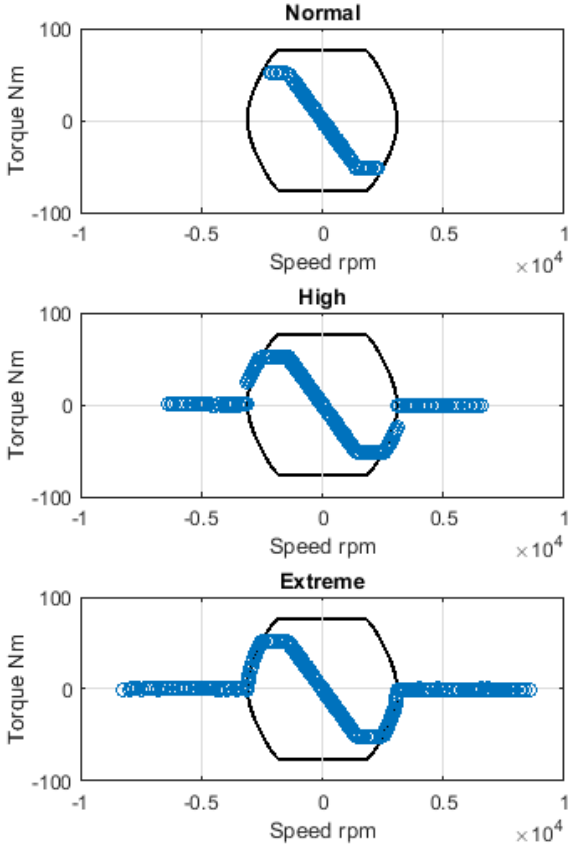

Fig. 12 Comparison of old generator torque-speed operating region (black line) and actual operating points (blue circles) for the normal, high and extreme sea states.

Figs 12 and 13 compare the torque speed operating range of the old and new generator for the three sea-states. The straight-line trajectory indicates linear damping control. The flat top shows the torque-limiting mode to protect the gearbox. For the old generator, in Fig. 12, this was is lower than the peak generator torque. The curved envelope shows the voltage-limiting mode. Points along the speed axis outside this envelope show speed violation. The figures highlight that in the normal sea state, the PTO is operating within design limits. It also shows the significant increase in speed under extreme conditions, where electrical disconnection of the PTO is recommended. Over speed is managed better with the new generator, due to its wider field-weakening range.

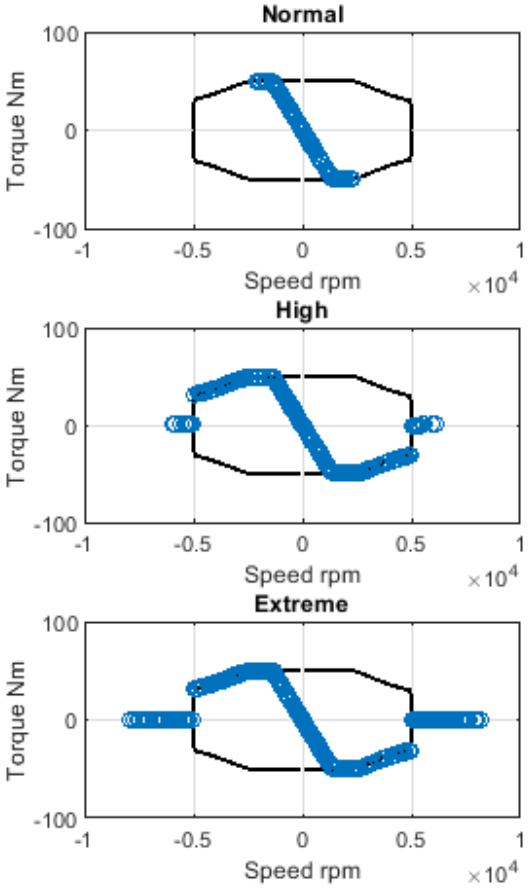

Fig. 13 Comparison of new generator torque-speed operating region (black line) and actual operating points (blue circles) for the normal, high and extreme sea states.

However, this is not the full picture. Table IV compares the power recovery from the two generators. The power recovery is similar for both generators in the nominal sea state, with the old generator recovering 3% more power. The new generator appears more effective in the high sea state, recovering 18% more power, but the constraint applied is for short-term peak current. Continuous current must also be managed to prevent the generator overheating. The rms current in Table IV is above the continuous rated value of the generator, listed in Table I, and would not be sustainable for more than a few minutes. Further work is required to adjust the constraints dynamically, according to the thermal state of the machine and the duration of the peak powers.

TABLE IV
POWER RECOVERY

Description	Sea state	Average power	Phase current
Old Generator	Nominal 0.5 m	1.43 kW	6.0 A
	High 1.0 m	4.06 kW	11.6 A
	Extreme 1.25 m	4.16 kW	13.7 A
New Generator	Nominal 0.5 m	1.39 kW	9.8 A
	High 1.0 m	4.72 kW	15.9 A
	Extreme 1.25 m	6.12 kW	17.4 A

VI. CONCLUSION

This paper has outlined the mathematical modelling and hardware design phases of a 20 m, kW scale, 121 M4 WEC which is due to go for sea trials in 2023/24. Only uni-directional waves have been considered in this paper. Average power figures should be treated with caution, as some loss mechanisms have been neglected in the PTO and the DC voltage control has been treated as ideal. The design stage has identified the current limit in the energy-storage isolation transformer as under-specified – this is a relatively low-cost item that can be upgraded. The gearbox has emerged as a more significant limiting factor for power scale-up. Field weakening range and both short-term and continuous current rating are important for the generator.

The models show that the specification of the generator and in particular the power-limiting constraints have a major effect on power recovery, so system co-design is important. The demonstrator platform uses an off-the-shelf machine, so is constrained by availability of products. The focus is on collecting operating data over a range of sea states, rather than long-term reliability. Work on appropriate setting of limits is ongoing, since inclusion of PTO losses and thermal conditions need measurements from future dry tests. Development of shutdown and re-start strategies when the speed limit is reached is ongoing. Future work will extend loss models and incorporate the DC link voltage regulation. Ultimately, the efficacy of the system can only be demonstrated in ocean conditions.

REFERENCES

[1] T. W. Thorpe, "A brief review of wave energy", *Energy Technology Support Unit (ETSU)*, Technical report no.R120, UK DTI," 1999

[2] C. Pérez-Collazo, D. Greaves, G. Iglesias, "A review of combined wave and offshore wind energy", *Renewable and Sustainable Energy Reviews*, Vol. 42, 2015, pp 141-153, doi:/10.1016/j.rser.2014.09.032.

[3] F. Mwasilu, J. W. Jung, "Potential for power generation from ocean wave renewable energy source: a comprehensive review on state-of-the-art technology and future prospects". *IET Renewable Power Generation*. 2019 Feb;13(3):363-75.

[4] B. Drew et al. "A Review of Wave Energy Converter Technology." *Proc. IMechE, Part A: Journal of Power and Energy*, vol. 223, no. 8, 2009, pp. 887–902.

[5] A. Babarit, "Ocean wave energy conversion: resource, technologies and performance". Elsevier, 2017.

[6] A. F. de O. Falcão, "Wave energy utilization: A review of the technologies." *Renewable and sustainable energy reviews,* 14, no. 3 (2010): 899-918.

[7] British Energy Security Strategy, H.M. Government, Apr. 2022.

[8] S. Pennock, H. Jeffrey, "UK power system benefits through deployment of marine energy technologies", *Supergen ORE Energy Policy Paper*, Jan 2023. Supergen-system-benefits-report-230323.pdf (supergen-ore.net) [Online]

[9] L. Kilcher, M. Fogarty, and M. Lawson, Marine "Energy in the United States: An Overview of Opportunities", *National Renewable Energy Laboratory, Technical Report* NREL/TP-5700-78773 Feb. 2021

[10] https://www.energy.gov/articles/doe-announces-25-million-cutting-edge-wave-energy-research [Online]

[11] https://blueeconomycrc.com.au/project/seeding-marine-innovation-in-wa-with-a-wave-energy-deployment-in-albany/ [Online]

[12] P. Stansby, E. C. Moreno, and T. Stallard, "Large capacity multi-float configurations for the wave energy converter m4 using a time-domain linear diffraction model," *Applied Ocean Research*, vol. 68, pp. 53–64, 2017

[13] Z. Liao, N. Gai, P. Stansby and G. Li, "Linear Non-Causal Optimal Control of an Attenuator Type Wave Energy Converter M4," *IEEE Trans. Sustainable Energy*, vol. 11, no. 3, pp. 1278-1286, July 2020, doi: 10.1109/TSTE.2019.2922782

[14] P. K. Stansby, E. Carpintero Moreno, "Hydrodynamics of the multi-float wave energy converter M4 with slack moorings: Time domain linear diffraction-radiation modelling with mean force and experimental comparison", *Applied Ocean Research*, Vol. 97, 2020, 102070, ISSN 0141-1187, https://doi.org/10.1016/j.apor.2020.102070.

[15] A. Kurniawan et al. "Numerical modelling in the development of the m4 prototype for Albany, western Australia". In *Proc. ASME 2023 42nd Int. Conf. on Ocean, Offshore and Arctic Engineering OMAE2023*, Melbourne, Australia, June 11–16,

[16] M. C. Sousounis et al., "Direct drive wave energy array with offshore energy storage supplying off-grid residential load". *IET Renewable Power Generation*. 2017 Jul;11(9):1081-8

[17] P. Moreno-Torres et al, "Power smoothing system for wave energy converters by means of a supercapacitor-based energy storage system". In Proc*17th European Conf. Pwr. Electron. and Apps. (EPE'15 ECCE-Europe)*, 2015, Sep 8 (pp. 1-9). IEEE

[18] S. Hazra and S, Bhattacharya, "Hybrid energy storage system comprising of battery and ultra-capacitor for smoothing of oscillating wave energy". In *Proc. 2016 IEEE Energy Conv. Congress and Exposition (ECCE)*, 2016 Sep 18 (pp. 1-8). IEEE

[19] T. Kovaltchouk et al., 2014. "Enhanced aging model for supercapacitors taking into account power cycling: Application to the sizing of an energy storage system in a direct wave energy converter", *IEEE Trans. Ind. Apps*, 51(3), pp.2405-2414.

[20] J. Aubry, H.B. Ahmed, H.B. and B. Multon, "Sizing optimization methodology of a surface permanent magnet machine-converter system over a torque-speed operating profile: Application to a wave energy converter", *IEEE Trans. Ind. Electronics*, 59(5), pp.2116-2125, 2011.

[21] Z. Sun el al., "Analytical prediction of the short-circuit current in fault-tolerant PM machines", *IEEE Trans. Ind. Electronics*, 55(12), pp 4210-7, 2008.

[22] Y. Zbede, and J. Apsley. "Field weakening control of a PM vehicle drive." *Journal of Engineering*, 2019.17 (2019): 3510-3515

[23] X. Zhang, J. Apsley and M. Iacchetti, "Computationally-efficient Modelling of Wave Energy Conversion Systems via Pseudo Steady-State PMSM model", In Proc. *11th Int. Conf. Power Electronics*, (*ICPE)*, 2023.

[24] S. Shao et al, "Modeling and advanced control of dual-active-bridge DC–DC converters: A review, " *IEEE Trans. Power Electronics, 37*, no. 2 (2021): 1524-1547.